Modelling a Resonant Near Field Scanning Microwave Microscope (RNSMM) Probe

N. Smith[*1], K. Lees[1], A Gregory[1] and R. Clarke[1]
[1] National Physical Laboratory, Materials Division.
* Corresponding author: National Physical Laboratory, Hampton Road, Teddington, TW11 0LW, UK.
nadia.smith@npl.co.uk

Abstract: The current drive to go beyond the state of the art in novel near field scanning microwave microscope (NSMM) metrology at the micro scale, to make them capable of traceable measurements on functional materials, has led to the development of a finite element model of the probe of a resonant near field scanning microwave microscope (RNSMM). The model has been validated against an analytical solution. Different sample configurations were investigated to understand how imperfect geometry and non-uniform materials affect the capacitance and the resistance of the system. The modelling has proved to be a very useful tool to provide insight into the effects of likely imperfections in this measurement technique.

Keywords: Near field microscopy, probe, capacitance, dielectric properties.

1. Introduction

The development of traceable electromagnetic (EM) materials metrology to enable the uptake of new EM and functional materials by European industries, especially electronics and ICT-related industries, is of great importance for future growth. As part of a European Metrology Research Programme (EMRP) Joint Research Project 'EMINDA' [1], the UK's National Physical Laboratory (NPL) has undertaken leading edge research in this field seeking progress on two fronts: firstly the development of key advanced measurement techniques and secondly the provision of a broader infrastructure for EM materials metrology in Europe.

Within this framework, NPL's aim has been to go beyond the current state of the art in novel near field scanning microwave microscope (NSMM) metrology at the micro scale, with the intention of making them capable of traceable measurements on functional materials. This intention is being supported by the introduction of a wider range of modelling techniques for NSMM measurements.

A particular type of NSMM is a resonant near field scanning microwave microscope (RNSMM). A RNSMM consists of two parts: a microwave resonator that typically has dimensions of centimeters, and which can be of several different designs; and a probe that interacts with a dielectric material, whose dimensions are of the order of microns. Dielectric probes of this type can in principle be used to scan the surface complex permittivity of dielectrics, typically composites, electro-ceramics, semiconductors, and thin films such as graphene [2]. When the probe approaches the material the resonance of the system will be perturbed. The change in resonance will be related to the complex permittivity of the material and the distance between the material and the probe. This paper will discuss a finite element model of the probe of an RNSMM, which has been developed to account for the dielectric loss, the non-flatness and non-uniformity of specimens in RNSMM measurements, and to understand the probe/tip interaction of a RNSMM.

2. Description of the model

2.1 Geometry

A sketch of the geometry of the probe and sample in its simplest form is shown in figure 1. The probe is regarded as a perfect solid cylinder attached to a perfect solid sphere. It is assumed that the cylinder is sufficiently long that the resonator and other parts of the device can be neglected so that only the probe and the sample need to be considered.

The sphere is 0.1 mm in diameter. The cylinder is 0.08 mm in diameter and 3 mm long, but at the frequencies of interest the shaft length can be

taken to be 0.32 mm. The sample is a disc of 4 mm diameter and 2 mm thick.

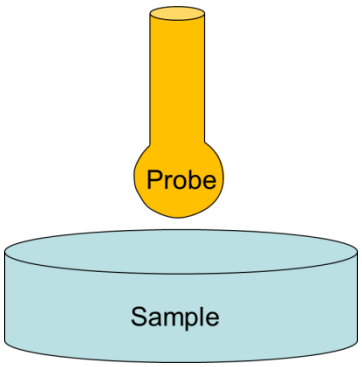

Figure 1: Sketch of probe and sample geometry. The probe is attached to a resonant cavity that need not be modelled.

The sample geometry as illustrated is flat and is a uniform material. Other sample configurations to be investigated are:

- Geometric imperfections: valley, hill.
- Layered materials: sample of finite thickness on a metal, film on top of a substrate.
- Inhomogeneous samples: a flat sample consisting of two distinct sections of differing materials.

The geometry of the system can be regarded as axisymmetric, as shown in figure 2. This assumption requires the axis of the probe to be aligned with the axis of the sample in all cases. It also places some limitations on how the alternative sample configurations listed above can be implemented:

- The valley and hill geometries have to either be centrally placed, or regarded as a circular ridge or trough in the sample;
- The inhomogeneous samples have to be structured as an inner cylinder of one material and an outer coaxial hoop of another material.

The probe and sample are encased in a box of air because the electric fields will propagate through air as well. A preliminary model showed that the sample is sufficiently wide that the box of air can be regarded as being above the sample only, and can have the same radius as the sample. The box of air entirely encloses the sphere. The outer limits of the box of air are shown as a red line in figure 2.

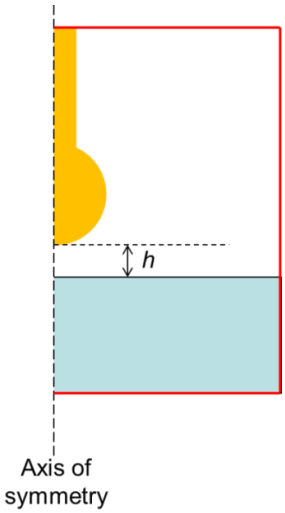

Figure 2: Simplified axisymmetric probe geometry, not to scale.

The probing process varies the gap between the probe tip and the sample, h. Gaps between 0 and 10 microns are of most interest and are studied in detail. A gap of 5 mm is also studied to test the assumption that this distance is sufficient to prevent the probe and the sample from interacting.

The valley and hill geometries are shown in figure 3. The two varying parameters are h and θ, where now h is the height of the bump below (or above) the surface, and θ the angle. The following values have been considered for h: 1, 3, 6, and 10 µm, and for θ: 30°, 60°, and 90°.

The two configurations of layered sample are shown in figure 4. Different cases have been set up with the values of r and t set to 1, 2, 5 and 10 times the probe radius (which is 0.05 mm), keeping the overall radius and thickness of the sample fixed. The value of t has also been set to 1 μm to set up a thin film model.

A high frequency alternating current is applied to the probe, which generates an electric field around the probe. This field is affected by the sample, and the effect can be sensed by looking at the current running through the probe. The aim

of this work is to understand how imperfect geometry and non-uniform materials affect the current.

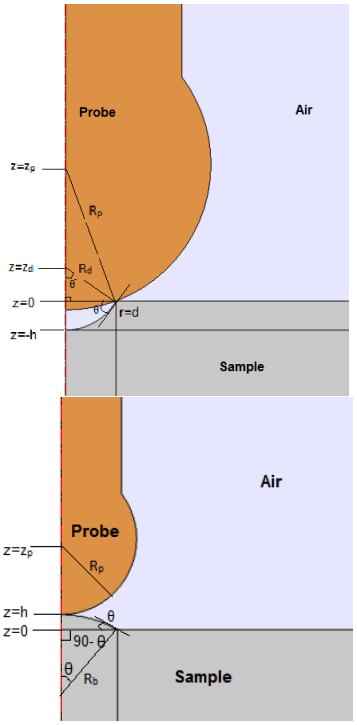

Figure 3: Configuration for the valley and hill geometries.

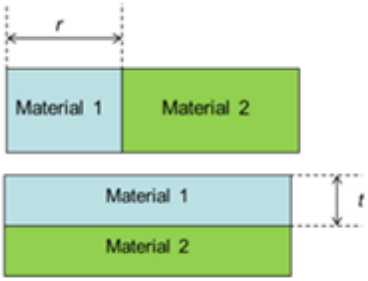

Figure 4: Configurations for the concentric and layered samples.

2.2 Governing equations

The equations to solve are that of the electric potential, *V*, together with the time-harmonic equation of continuity and a constitutive relation:

$$\mathbf{E} = -\nabla V$$
$$\nabla \cdot \mathbf{J} = -j\omega\rho$$
$$\mathbf{J} = (\sigma + j\omega\varepsilon_0\varepsilon_r)\mathbf{E} + \mathbf{J_e}$$

where $\mathbf{J}$ is the current density, $\mathbf{E}$ is the electric field, ρ is the charge density, ω is the angular frequency, ε_0 is the permittivity of vacuum, ε_r is the relative permittivity of the material, σ is the electrical conductivity of the material, and $\mathbf{J_e}$ is an externally generated current.

These equations are completed with the following boundary conditions:

- Terminal (i.e. V=1 V) on the top boundary of the probe.
- Ground plane (i.e. V=0 V) on the bottom of the sample.
- Electric insulation (i.e. $\mathbf{n} \cdot \mathbf{J} = 0$) everywhere else.

3. Use of COMSOL Multiphysics

This work required the use of the AC/DC module of COMSOL, specifically the electric currents capability in the frequency domain. The high frequency alternating current is applied to the probe using the terminal node, which generates an electric field around the probe. The use of a terminal node enabled the computation of the lumped parameters of the system, such as the capacitance and resistance.

The frequencies at which the model has been run are 240 MHz, 1.5 GHz, and 3.9 GHz, which correspond to the operating frequencies of the NPL RNSMMs. The mesh in the gap between the sphere and the sample, and in the first few microns of the sample, needs to be very fine. For this special mesh, commands and a subdivision of the geometry were set up to make it easy to focus on this area.

3.1 Validation against analytical model

There is an analytical solution to the problem [3] if the probe is treated as a sphere (no cylinder) in contact with a sample which is uniform and perfectly flat. This solution has been used to compare to the numerical one obtained in COMSOL.

In the validation the sphere and sample have the same dimensions as those mentioned above, and the sample is taken to have relative permittivity

3.8 and conductivity 0. The sphere is considered to be copper (thus using COMSOL's inbuilt properties for copper).

The results of interest for the initial model are the z component of the electric field in the first few microns of the sample along the axis of symmetry. These results have to be compared with values of the electric field calculated from expression (2) in [3], which is:

$$\vec{E} = \frac{q}{2\pi(\epsilon+\epsilon_0)} \sum_{n=1}^{\infty} \frac{1}{n} b^{n-1} \frac{r\overrightarrow{e_r} + \left(z+\frac{R_0}{n}\right)\overrightarrow{e_z}}{\left[r^2+\left(z+\frac{R_0}{n}\right)^2\right]^{\frac{3}{2}}},$$

where $b = (\epsilon - \epsilon_0)/(\epsilon + \epsilon_0)$, ϵ is the relative permittivity, ϵ_0 is the permittivity of free space; $q = 4\pi\epsilon_0 R_0 V_0$, R_0 is the radius of the tip, V_0 is open end peak voltage; $\overrightarrow{e_r}$ and $\overrightarrow{e_z}$ are the unit vectors along the directions of the cylindrical coordinates r and z, respectively.

Figure 5 shows excellent agreement between the electric field values calculated numerically and analytically in the first 50 μm along the axis of symmetry.

Once the model had been validated against the analytical solution, the different sample configurations described above were investigated to understand how imperfect geometry and non-uniform materials affect the capacitance and the resistance. For all geometries, different material permittivities were considered to address the full range (relative permittivity ranging from 1 to 1000) seen in real materials.

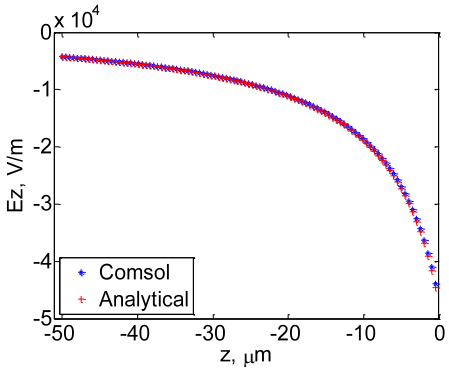

Figure 5: Comparison of numerical and analytical solution for a case of a spherical probe in contact with a homogeneous sample with a flat surface.

4. Results and discussion

All of the different cases described above have been simulated using COMSOL. For each of the models, the capacitance between the probe and sample has been calculated. As the probe is small compared with the microwave wavelength, the capacitance is effectively frequency independent, so for all the frequencies run the results are found to be the same. Comparisons have been made between the different scenarios.

Figure 6 shows how the capacitance changes with h (distance between sample and probe) for a lossless uniform material with a flat surface. The difference caused by changing the permittivity can also be seen as each coloured line corresponds to a different permittivity value. It can be seen that capacitance decreases as h increases and as permittivity decreases. It should be noted that the 5 mm values for the different permittivities have not converged to a single value, which indicates that even at this distance the probe is interacting significantly with the sample – a significant finding for practical measurements.

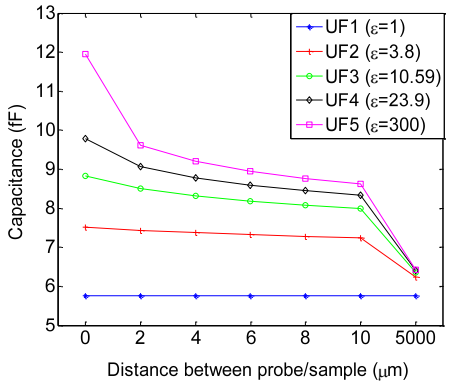

Figure 6: Capacitance results for a uniform material with a flat surface, as a function of h. Different colours correspond to different material permittivity.

Figure 7 shows the capacitance variation as a function of h for a concentric material. The different coloured lines correspond to different radii of the inner material, M1. Also included are the cases "All M2" and "All M1" which are the capacitance calculated for uniform materials M2 and M1, respectively. In this particular case M1

has a relative permittivity value of 3.8, and M2 is taken to be copper. This type of graph can be

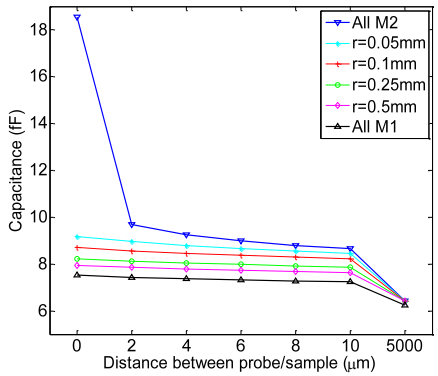

Figure 7: Capacitance results for a concentric material, as a function of *h*. Different colours correspond to different ratios between materials 1 and 2.

Figure 8 shows the capacitance variation for several tests run on the hill (plots on the left) and valley (plots on the right) geometries for uniform materials with different relative permittivity values (along the x-axis). For all of these tests the probe was in contact with the sample, and the variation is in the angle and height of the hill (or valley) off (or into) the surface (as shown in figure 3). The upper plots correspond to a hill or a valley of 1 μm height, and the lower plots to that of 6 μm. The different coloured lines correspond to different angles off (or into) the surface. The black line on all the plots corresponds to a flat surface sample, included for comparison purposes. As can be seen, the capacitance of the hill surfaces is lower than that of a flat surface, whilst it is higher for the valley surfaces. For a hill of 1 μm height off the surface, the angle does not affect the capacitance significantly; whilst for the 6 μm height hill, the lower the angle the closer the capacitance is to that of a flat surface. On the other hand, for a valley surface, the lower the angle the furthest the capacitance is to that of a flat surface. Again, for 6 μm valley the differences are more pronounced than for a 1 μm valley.

For lossy dielectrics, for which the imaginary permittivity, ϵ", is non-zero, an informative way of presenting the data from these simulations is via a mapping from the complex permittivity plane to the complex capacitance plane – where used to see how large *r* should be to ignore the effects of material 2 on material 1.
the permittivity, ϵ' - jϵ", is the complex permittivity of the dielectric and the 'complex capacitance' is just a way of presenting the complex admittance seen by the probe: $Y = G + j\omega C$. The complex capacitance C* is defined as $C^* = C' - jC''$, where $C' = C$ and $C'' = G/j\omega$. These mappings enable one to read off the material complex permittivity corresponding to a given (notionally measured) complex capacitance.

Mappings of this kind are shown in figures 9 and 10. In both figures the horizontal (black) axis corresponds to C' and the vertical axis corresponds to C". In both figures ϵ' on the mapping increases as one moves to the right. Figure 10 plots ϵ" vertically on the mapping, while figure 9 uses an alternative representation of dielectric loss, the loss tangent, tan δ, defined as ϵ''/ϵ' (tan δ is a parameter commonly used by electrical engineers to represent dielectric loss).

Both figures demonstrate how useful this form of modelling and mapping can be. For example, it is clearly shown that the real capacitance, C', is affected by dielectric loss, ϵ" or tan δ. This is a feature which simple capacitive models of probe/sample interaction cannot capture.

5. Conclusions

The modelling presented in this work has proved to be a very useful tool to provide insight into the effects of likely imperfections in the real measurement technique. Modelling studies of this kind can help answer questions which will help with the experiments such as: how accurately does the separation between the probe and the sample need to be known; how flat does the surface need to be; if the sample is composed of two materials, how accurately can the permittivity of either of them be measured?

The work has further shown that simple capacitive models of probe/sample interaction cannot capture many of the effects described above, and this fact in turn demonstrates the importance of this form of modelling for RNSMM metrology to be made fully traceable.

6. References

1. EMINDA project website http://projects.npl.co.uk/eminda/

2. Andrew Gregory, Ling Hao, Norbert Klein, John Gallop, Cecilia Mattevi, Olena Shaforost, Kevin Lees, and Bob Clarke, *Spatially resolved electrical characterisation of graphene layers by an evanescent field microwave microscope*, *Physica E* (2012), http://dx.doi.org/10.1016/j.physe.2012.10.006

3. C. Gao and X.-D. Xiang, Quantative microwave near-field microscopy ofdielectric properties, *Review of Scientific Instrument, 69 (11), 3846-3851 (1998).*

7. Acknowledgement

This project was funded by the 'EMINDA' EURAMET joint research project which received its funding from the European Community's Seventh Framework Programme, ERA-NET Plus. The authors would like to thank their partners in the EMINDA project for valuable discussions on these issues, and L. Wright of NPL for guidance on the modelling.

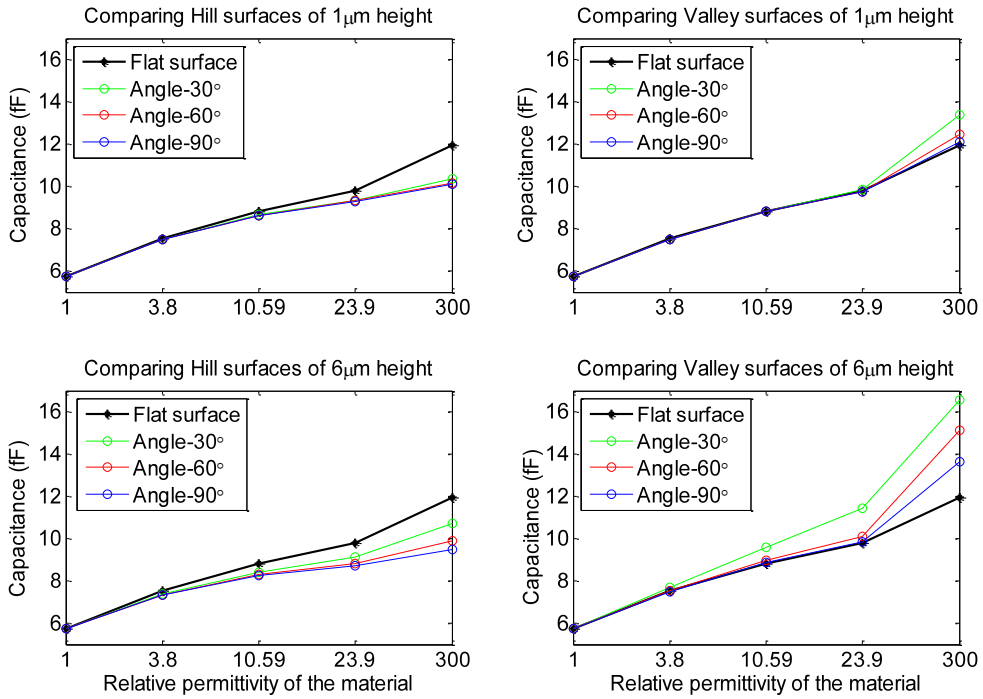

Figure 8: Capacitance results for uniform materials with different permittivities (along x-axis) with hill (left) or valley (right) geometries. The top plots correspond to a hill or a valley of 1 μm height, and the bottom plots to 6 μm. The different colours correspond to different angles off (or into) the surface. The probe is in contact with the sample for all of these cases.

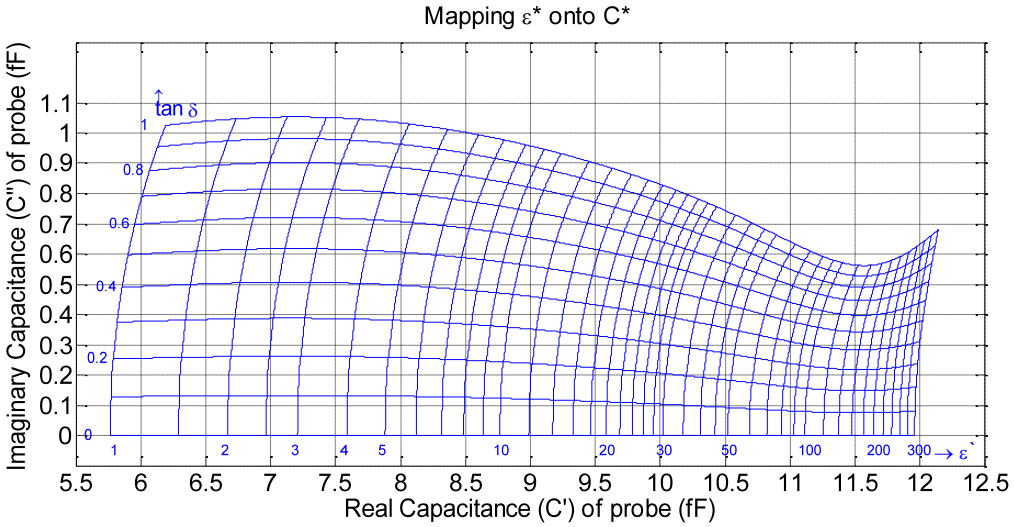

Figure 9: Mapping from the complex permittivity plane to the complex capacitance plane, for a range of relative permittivity values from 1 to 300. The material considered is uniform and has a flat surface. The probe is in contact with the sample for all of these cases.

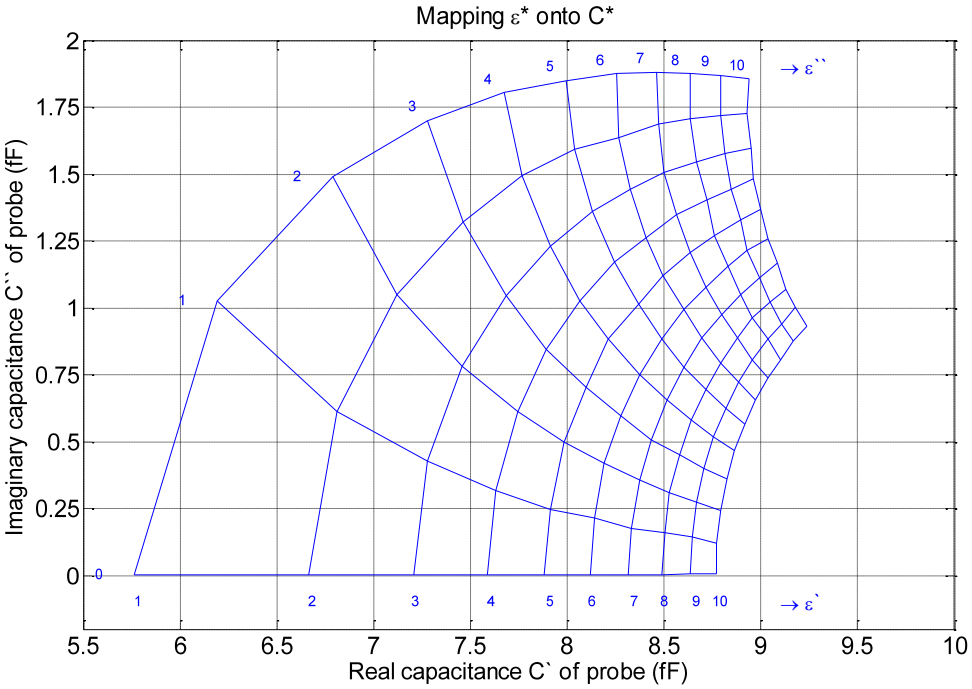

Figure 10: Mapping from the complex permittivity plane to the complex capacitance plane for a range of relative permittivity values from 1 to 10. The material considered is uniform and has a flat surface. The probe is in contact with the sample for all of these cases.